Computational Thermal Sciences, 4 (2): 137-149 (2012)

1D AND 2D MODELING AND SIMULATION OF RADIAL COMBUSTION PROPAGATION ON Fe_2O_3/Al THERMITE SYSTEMS

P. Brito,[1,2] L. Durães,[1,*] & A. Portugal[1]

[1]*CIEPQPF, Department of Chemical Engineering, Faculty of Sciences and Technology, University of Coimbra, Pólo II, Rua Sílvio Lima, 3030-790 Coimbra, Portugal*

[2]*Department of Chemical and Biological Technology, School of Technology and Management, Polytechnic Institute of Bragança, Campus de Santa Apolónia, PO Box 1134, 5301-857 Bragança, Portugal*

[*]Address all correspondence to L. Durães E-mail: luisa@eq.uc.pt

In previous works, a one-dimensional model was built to simulate the nonsteady radial combustion propagation on thin disk-shaped samples of Fe_2O_3/aluminum thermite mixtures and was successfully tested. Now, the purpose is to extend the referred model to the more sensible two-dimensional features of the samples, maintaining the main characteristics of the previous model: zero-order kinetics, conductive/radiative heat transfer, assumption of phase transitions, temperature and composition dependency for all system properties during propagation. Therefore, an adaptive numerical algorithm that conjugates a method of lines (MOL) strategy based on finite differences space discretizations, with a collocation scheme based on increasing level dyadic grids is applied for the solution of the problem. The particular integration method proves to cope satisfactorily with the steep traveling thermal wave in 1D and 2D spatial domains, either for trivial uniform mixing conditions, as in complex examples developed to feature more sophisticated circumstances, such as nonhomogeneous reactant mixing, which realistically replicate the observed experimental conditions.

KEY WORDS: *combustion, Fe_2O_3 aluminum thermite, modeling, adaptive methods, finite differences, method of lines, dyadic grids, nonhomogeneous mixtures*

1. INTRODUCTION

The self-propagating high-temperature reactions, such as the Fe_2O_3/aluminum thermite combustion, are difficult to follow by experimentation due to fast chemical and physical transformations and the high temperatures achieved. Consequently, studies concerning theoretical prediction of these combustion processes have been published (Moore and Feng, 1995; Makino, 2001) and represent a valuable guideline for experimental work.

The Fe_2O_3/aluminum thermite reaction has already been simulated in cylindrical geometry with a one-dimensional coordinate system attached to the uniformly propagating combustion wave (Raymond et al., 1998; Shkadinsky et al., 1997, 2000), and with a fixed one-dimensional coordinate system (Brito et al., 2004). The availability of experimental data for radial combustion on disk shaped samples (Durães et al., 2006a) has stimulated, in an earlier work, the derivation of a one-dimensional model to describe the Fe_2O_3/Al radial combustion propagation (Brito et al., 2005). The main features of this model are presented in the next section. The combustion front propagation velocity, temperature, and final products composition were obtained, solving the model with an adaptive numerical scheme, and the solution numerical profiles proved to be fast moving steep fronts, which were validated by experimental results (Durães et al., 2006b; Brito et al., 2007).

Our particular interest resides in a general strategy for the solution of partial differential equations (PDEs), named "method of lines" (MOL) (Schiesser, 1991); its structure can hold various schemes of mesh discretization.

1940–2503/12/$35.00

NOMENCLATURE

a	spatial interval lower-boundary position
b	spatial interval higher-boundary position
C_{P}	heat capacity [J/(kg K)]
k	thermal conductivity [W/(m K)]
K	zero-order kinetic constant [kg/(m^3 s)]
L	latent heat (J/kg)
M	lower-resolution grid level
N	higher-resolution grid level
N_{int}	number of intervals of the lower-resolution 1D grid
N_{Ref}	maximum refinement level
P	pressure (Pa)
Q	reaction heat (J/kg)
$\Re$	reaction kinetic rate [kg/(m^{3}s)]
r	radial coordinate (m)
R	sample radius (m)
R_0	ignition zone radius (m)
t	time coordinate (s)
T	temperature (K)
T_{igni}	ignition temperature (K)
T_{react}	reaction temperature (K)
T'	temperature normalization constant (K)
U, U'	heat transfer coefficient [W/(m^2 K)]
U_i^n	derivative approximation of degree n at internal grid position i
W	mass concentration (kg/m^3)
v	radial combustion propagation velocity (m/s)
Z	sample thickness (m)

Greek Symbols

α	mass stoichiometric coefficient
β_1, β_2	numerical collocation algorithm control parameters
ε	emissivity
ϕ	angular coordinate
ρ	density (kg/m^3)
σ	Stefan-Boltzmann constant W/(m^2·K^4).
τ	time normalization constant (s)
υ	volume fraction
ω	mass fraction

Subscripts

M	mixture conditions
i	arbitrary component
A	Fe_2O_3
B	Al
C	Fe
D	Al_2O_3
E	air
PMMA/air	PMMA interface
steel/air	steel interface
x	first spatial coordinate
y	second spatial coordinate
0	initial or surrounding conditions

Usually, the numerical solution of PDEs implies the approximation of the original differential continuous problem to a system of algebraic equations defined on a discrete domain. This transformation may be done simultaneously along every independent variable, or a two-stage strategy may be applied: First, the discretization of the original problem in all directions but one (normally time for initial-boundary value problems) and, second, the integration in the remaining direction using a standard integrator package. The initial PDE problem is approximated to a system of ordinary differential equations (ODEs) that can be solved by an available ODE integrator. Hence, one can resort to a wide variety of different basis functions to execute the discretization step, e.g., Taylor expansion approximations (Schiesser, 1991), different-order polynomials, wavelets (Santos et al., 2003; Cruz et al., 2003), radial basis functions (Driscoll and Heryudono, 2007), etc.

The typical approach to the referred procedures is rigid and nonadjustable to its evolution. One way to overcome the possible problems that may arise from this lack of flexibility is the adoption of the adaptation concept. Adaptivity implies the tuning of algorithm parameters to the particular conditions of the solution evolution.

In the PDE solving field, the objectives of the adaptive procedures have always been the same: To generate grids that gather nodes in the domain regions where the solution is more active (i.e., exhibits steeper gradients) and disperse them in the remaining areas, and/or follow efficiently the problematic features of the solution. The introduction of the concept of adaptivity into

the wider MOL procedure is a fairly straightforward operation (Vande Wouwer et al., 2001).

In the present work we chose to construct an adaptive grid based on a series of embedded dyadic grids of increasing level, at each time step of the integration. A *k*-level one-dimensional uniform dyadic grid is defined by a nodal mesh with 2^k equidistant intervals. Therefore, a higher-level grid is generated by adding nodes to the previous one, at every interval center position (see Fig. 1). It is important to note that a grid of level *k* is always included in all grids of higher level. The principle is to construct grids that merge nodes of different resolution levels according to the estimative of the function activity over the different regions of the whole domain. This is accomplished by the definition of a collocation criterion. The referred approach can be rather easily extended to two-dimensional dyadic grids (see Fig. 2). Hence, we established a collocation strategy that applies function-dependent features, allowing the activation (or deactivation) of nodes belonging to dyadic grids ranging from a minimum resolution level (*M*) to a maximum resolution level (*N*). Then, we introduce this strategy for the generation of spatial grids, in an overall MOL algorithm devised for the adaptive numerical solution of one- and two-dimensional evolutionary PDE systems, considering the case study of Fe_2O_3/Al thermite combustion. For this chemical system, we used the experimental results for the radial combustion propagation velocities and temperature from an earlier work to fit the model kinetic constant and also for comparison with the calculated velocity profiles.

2. MODEL

2.1 1D Model

The 1D model was already presented in Brito et al. (2005, 2007) and Durães et al. (2006b), and is based on the following general assumptions: (i) one-dimensional radial nonsteady propagation; (ii) general reaction with mass stoichiometry $\alpha_A A+\alpha_B B\rightarrow \alpha_C C+\alpha_D D$ and limiting reactant A; (iii) pseudo-homogeneous approach for the volume element, but considering the contribution of air to simulate a porous medium; (iv) zero-order kinetics; (v) conductive/radiative heat transfer mechanisms; (vi) negligible relative movement between species; (vii) sample geometry and dimensions; (viii) nonadiabatic system considering the confinement materials' properties and environmental conditions.

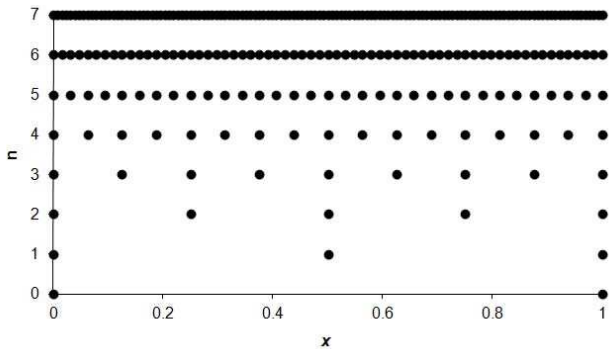

FIG. 1: Uniform 1D dyadic grids of increasing level.

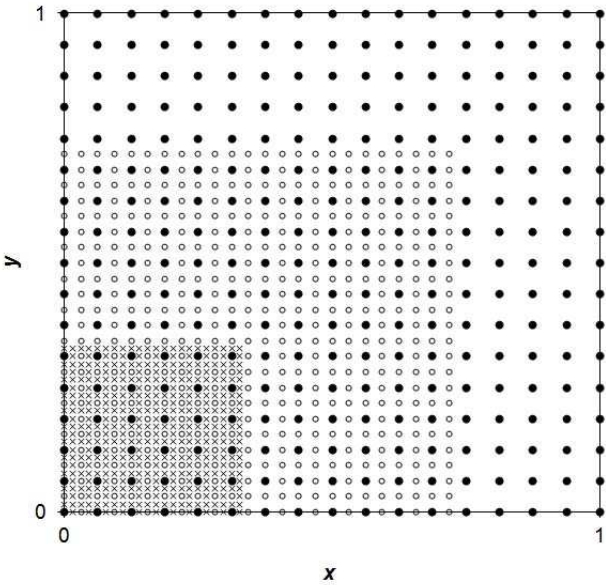

FIG. 2: Uniform 2D dyadic grids of increasing level.

The energetic and mass partial balances become

$$\rho_M C_{PM}\frac{\partial T}{\partial t}=\frac{1}{r}\frac{\partial}{\partial r}\left[k_M\left(r\frac{\partial T}{\partial r}\right)\right]+Q\cdot\Re - \left[\left(U_{steel/air}+U_{PMMA/air}\right)(T-T_0)+2\sigma\varepsilon_M \times\left(T^4-T_0^4\right)\right]/Z \quad (1)$$

$$\frac{dW_A}{dt}=-\alpha_A\Re \quad (2)$$

where W_A is the mass concentration of the limiting reactant (Fe_2O_3). The reaction enthalpy, $-Q(T)$ is computed considering the enthalpy variations [$C_P(T)$ integral and phase transitions] at constant pressure of reactants and products in the temperature path: $T_0 \rightarrow T$. The reaction kinetics is defined by $\Re = \boldsymbol{H}(T-T_{react})\,K$, where $\boldsymbol{H}$ is the

Heaviside function and K a non-temperature-dependent kinetic constant. This constant is adjusted for each specific chemical system considering the stationary combustion propagation velocity observed experimentally (see Section 3). The last term in Eq. (1) accounts for heat losses through the sample top and bottom to the surrounding (at T_0). The differential problem is completed by the definition of initial and boundary conditions:

$$t = 0 \quad \begin{cases} 0 \le r \le R_0 \quad \Rightarrow \quad T = T_{\text{igni}} \\ r > R_0 \quad \Rightarrow \quad T = T_0 \end{cases} \tag{3}$$

$$t > 0; \quad r = 0 \quad \Rightarrow \quad \frac{\partial T}{\partial r} = 0 \tag{4}$$

$$t > 0; \quad r = R \quad \Rightarrow \quad k_{\text{M}} \frac{\partial T}{\partial r} = -\left[U'_{\text{steel/air}} \left(T - T_0\right) + \sigma \varepsilon_{\text{M}} \left(T^4 - T_0^4\right)\right] \tag{5}$$

Equation (3) simulates ignition by a temperature spatial pulse with height T_{igni} and length R_0 at the initial time. On the inner and outer boundaries, a symmetry condition and conductive/radiative heat transfer are considered, respectively.

The thermophysical properties are allowed to vary with the temperature and composition of the mixture. The mixing rules for each property, to obtain the averaged mixture properties (mixture properties) for the pseudo-homogeneous volume element, are:

$$C_{\text{PM}} = \sum_i \omega_i C_{\text{P}i}; \quad \rho_{\text{M}} = 1 \Big/ \sum_i \frac{\omega_i}{\rho_i};$$
$$k_{\text{M}} = \left(1 \Big/ \sum_i \frac{\upsilon_i}{k_i} + \sum_i \upsilon_i k_i\right) \Big/ 2; \; \varepsilon_{\text{M}} = \sum_i \upsilon_i \varepsilon_i \tag{6}$$

where ω_i and υ_i are the mass and volumetric fractions of component *i*, being *i* = A, B, C, D, and E. The pseudo-homogeneous approach can be justified, in these heterogeneous condensed systems with self-propagating high-temperature reactions; since the reaction zone width (millimeters) is usually much larger than the heterogeneous scale of the medium (particles with micrometric size), the melting and homogenization phenomena that occur help to give consistency to this approximation (Varma and Lebrat, 1992; Mukasyan et al., 1996, 1999; Varma et al., 1998; Durães, 2007).

The mixture conductivity was taken as the average value between the conductivity of a serial and a parallel rearrangement of the components on a very narrow film (thickness Δr) centered on each spatial node position. An equivalent conductivity component is introduced in air conductivity estimative ($k'_{\text{E}} = k_{\text{E}} + 4\sigma\varepsilon_{\text{M}} T^3{}_{\text{E}} \Delta r$), for the radiation on the void spaces of the serial arrangement, since this phenomenon is significant above 200°C (Tavman, 1996; Gonzo, 2002). This thermal conductivity model was developed by the conjunction of ideas/models found in the literature to define the effective thermal conductivity for several types of composite solid matrices (Jakob, 1949; Bowen and Derby, 1995; Tavman, 1996; Gonzo, 2002). The introduction of air in the mixture had two main purposes: (i) approximating the mixture properties to those of a porous mixture; for instance, reducing the material density; (ii) introducing the radiation phenomenon equivalent to that existing in the transparent voids, which is of major importance for the heat transfer in the energetic composite. Of an experimental point of view, the voids also induce an increase of the specific surface area of the material, enhancing its reactivity, an increase of the combustion intensity in the voids' boundaries due to the radiation effect, and an increase in the turbulence/mixing of melted reactants. Although the developed approach still is simplified, as it is based on pseudo-homogeneous volume elements and thus it cannot take into account part of these effects, it constitutes an added value of the present combustion model in relation to the major part of the models found in the literature for this kind of reactions (see Durães, 2007).

Phase transitions of the components are also considered in the model, over a temperature range (ΔT) of 1 K, each time its transition temperatures are crossed, by means of an equivalent C_{P}: $C'_{\text{Pi}} = C_{\text{Pi}} + L_i/\Delta T$ (L_i is latent heat).

The thermophysical properties of the components and their dependencies with temperature were given in Brito et al. (2005), as well as the confinement materials' properties.

The model solution comprises temperature and composition spatial and temporal profiles. The composition profiles were used to estimate the combustion wave propagation velocity, considering the front position vs time. The location of the front was obtained by localizing the position of the 50% conversion point.

2.2 2D Model

The 2D model defined over a cylindrical reference system was constructed by adding the angular direction to the 1D model described above. Therefore, the energetic balance becomes

$$\rho_{\mathrm{M}} C_{\mathrm{PM}} \frac{\partial T}{\partial t} = \frac{1}{r}\frac{\partial}{\partial r}\left[k_{\mathrm{M}}\left(r\frac{\partial T}{\partial r}\right)\right] + \frac{1}{r^2}\frac{\partial}{\partial \phi}\left(k_{\mathrm{M}}\frac{\partial T}{\partial \phi}\right) + Q\cdot\Re - \left[\left(U_{\mathrm{steel/air}} + U_{\mathrm{PMMA/air}}\right)(T - T_0) + 2\sigma\varepsilon_{\mathrm{M}}\left(T^4 - T_0^4\right)\right]/Z \quad (7)$$

and the correspondent boundary conditions are

$$t > 0;\ r > 0 \ \Rightarrow \begin{cases} T(\phi = 0) = T(\phi = 2\pi) \\ \dfrac{\partial T}{\partial \phi}(\phi = 0) = \dfrac{\partial T}{\partial \phi}(\phi = 2\pi) \end{cases};$$

$$r = 0 \Rightarrow \quad \frac{\partial T}{\partial \phi} = 0 \quad (8)$$

These conditions represent the coincident and continuously differentiable nature of radial profiles for angular positions ϕ = 0 and ϕ = 2π, and the nonvariability of properties on the sample center position (r = 0) for all ϕ coordinates.

3. NUMERICAL METHODS

3.1 Adaptive Collocation Strategy

Using the concept of dyadic grid associated with finite differences approximations, we constructed a collocation algorithm for grid generation which can be applied in a MOL algorithm general context. For instance, consider a region of the spatial domain defined by two consecutive one-dimensional dyadic grids [see Fig. 3(a)]. A collocation algorithm is devised for the activation of nodes by the scheme presented in Fig. 3(b) (Brito, 2010). Using the local mesh size computed by

$$\Delta x = \frac{x_{i+1}^k - x_{i-1}^k}{2} \quad (9)$$

we created a criterion that intends to identify oscillations on the finite difference approximation of degree *n* at each internal grid position *i* (U_i^n)—criterion C1; alternatively, a second criterion is defined which tracks high variations on the finite difference 1D profile—criterion C2 (see Table 1). A criterion C1σ was also developed, by the substitution of the average evaluation presented above by a standard deviation test.

β_1 and β_2 represent the criteria tolerances that control the sensibility of the process to the identification of nonuniformities in the solution numerical profiles. The grid resolution is increased by the activation of higher-level nodes that do not verify the collocation criteria. The set of all active nodes over each dyadic grid generates the overall adaptive grid.

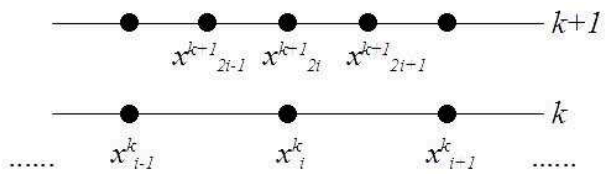

(a)

1. $k = M$
2. **for** $i = 1, \ldots, 2^k - 1$
3. estimate U_i^n (order *n* derivative at node *i*) by finite differences
4. **if** collocation criterion is met: select intermediate nodes of level k+1: $x_{2i-1}^{k+1}; x_{2i}^{k+1}; x_{2i-1}^{k+1}$
5. $k = k + 1$ (repeat **for** $k = M, \ldots, N - 1$)

(b)

FIG. 3: Representation of the **(a)** connection between nodes of consecutive 1D levels and **(b)** collocation algorithm for the activation of nodes.

TABLE 1: Collocation criteria for adaptive 1D grid generation

Criterion C1	compute $\delta_1 = U_i^n \times U_{i-1}^n$ and $\delta_2 = U_{i+1}^n \times U_i^n$ criterion verified if: $\lvert U_i^n \times \Delta x\rvert > \beta_1$ or $\begin{cases} \delta_1 \le 0 \\ \delta_2 \le 0 \end{cases}$ and $\dfrac{\lvert U_{i-1}^n\rvert + \lvert U_i^n\rvert + \lvert U_{i+1}^n\rvert}{3} > \beta_2$
Criterion C2	compute $\delta_1 = U_i^n - U_{i-1}^n$ and $\delta_2 = U_{i+1}^n - U_i^n$ criterion verified if: $\lvert U_i^n \times \Delta x\rvert > \beta_1$ or $\delta_1 \times \delta_2 \le 0$ and $\dfrac{\lvert\delta_1\rvert + \lvert\delta_2\rvert}{2} > \beta_2$

The collocation algorithm described above may be easily extended to 2D domains by a wide variety of strategies. We chose to select a specific scheme named C52, which is based on a 2D domain sweeping, by sequencing 1D procedures over the 1D-*x* grids for each higher-resolution level *y* position, followed by similar procedures on the correspondent 1D-*y* grids at the higher-resolution *x* positions, as described in Brito (2010).

3.2 1D Algorithm

The node collocation procedure is incorporated in an algorithm for the resolution of one-dimensional time-dependent PDE's. This strategy is based on the conjugation of a MOL algorithm where the space derivatives are approximated by finite differences formulas or high-resolution schemes (HRS), with grid generation procedure at specified times that reformulate the space grid according to the solution evolution (see Fig. 4). At these intermediate times the solution profiles are reconstructed through an interpolation scheme. The time integration can be performed by the ODE integrators DASSL (Petzold, 1982) or RKF-45 (Shampine et al., 1976). Therefore, the presented algorithm can be included in the class of *h*-refinement (static regridding) PDE solution adaptive procedures. The finite difference coefficients are computed using the recursive method of Fornberg (Fornberg, 1988), the HRS schemes are based on the NVSF method (Darwish and Moukalled, 1994) associated to flux limiting strategies, such as SMART or MINMOD procedures (Alves et al., 2003), and the interpolation step is done by linear or cubic splines approximations.

3.3 2D Algorithm

The collocation algorithm described above was also adapted for its application in the solution of 2D models over 2D dyadic grids of which the hierarchical relation is presented in Fig. 5. This algorithm (see Fig. 6) is similar to the 1D procedure depicted in the preceding section, the most important differences being related to the need of developing an interface which translates the 2D original problem into a 1D support for introduction in the time

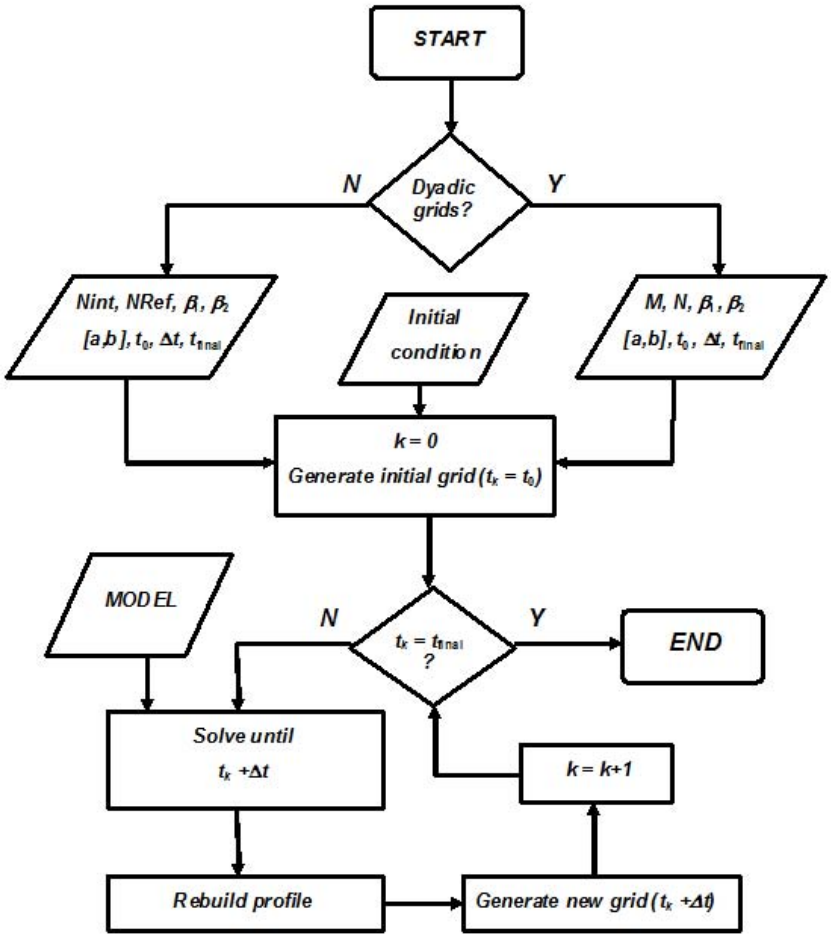

FIG. 4: General flow sheet for the 1D integration algorithm.

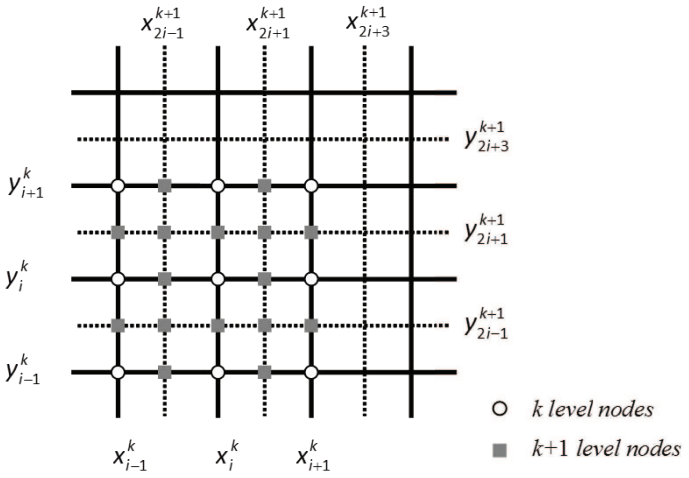

FIG. 5: Representation of the connection between nodes of consecutive 2D levels.

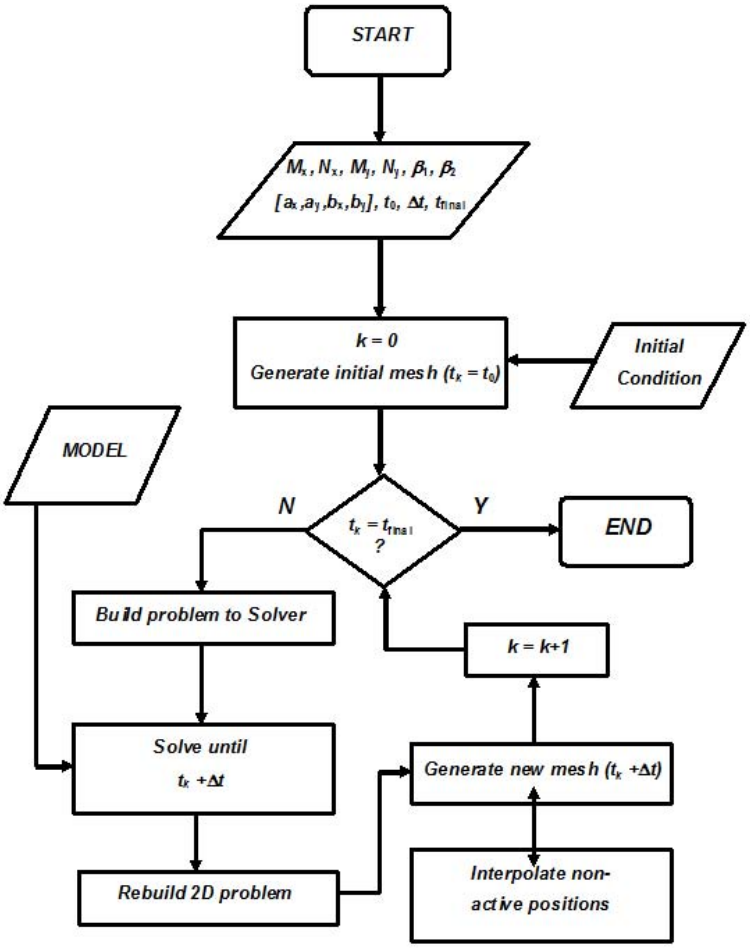

FIG. 6: General flow sheet for the 2D integration algorithm.

integrator followed by the corresponding 2D problem reconstruction after the integration step.

4. EXPERIMENTAL

Industrial Fe_2O_3 (1.7 μm, 96%, Bayer) and aluminum (18.6 μm, 89.3%, Carob) powders were mixed in stoichiometric ratio, following the reaction scheme of Eq. (10). Chemical and physical characterization of reactants, and the mixtures preparation procedure were presented in previous papers (Durães et al., 2006a, 2007).

$$Fe_2O_3 + 2Al \rightarrow 2Fe + Al_2O_3 \tag{10}$$

Reactant mixtures were compressed in a stainless steel circular box with an inner PMMA lid (Durães et al., 2006a). Samples combustion was initiated in an ignition central channel, via a nichrome wire instantaneously heated by a capacitor discharge. Radial flame propagation was monitored by digital video-chrono-photography. Combustion thermograms were registered at two different radii, using W/Re thermocouples.

Figure 7 presents an example of the video frames collected from the radial combustion propagation in one of the tested samples. From these frames, it was possible to draw the corresponding combustion front radial profiles (see Fig. 7), from which the radial combustion propagation velocities could be evaluated in four perpendicular axes of the samples (as later presented). With these data, the average combustion velocity for stationary propagation conditions (in the radii interval of 5–25 mm) was obtained: 0.0269±0.0022 m/s. The average temperature obtained with the thermocouples was ∼2300 K. Note that the radial combustion propagation profiles, velocities, and temperatures were more deeply discussed in Durães et al. (2006a).

5. RESULTS AND DISCUSSION

5.1 1D Model

First we defined the general system conditions. The purpose is to integrate a normalized version of the described 1D and 2D models, in which all process state and independent variables are normalized by suitable parameters. The conditions used in all 1D and 2D simulations are listed in Table 2 and the most of them were defined considering experimental conditions/measurements.

The 1D procedure described in Section 3 (see Fig. 4) was applied to the 1D model using the numerical conditions depicted in Table 3.

The numerical propagation results are presented in Figs. 8 and 9, for kinetic constant K = 80,000 kg·m^{-3}·s^{-1} with uniform mixing conditions for a stoichiometric reactant ratio. The given K value was the one that resulted

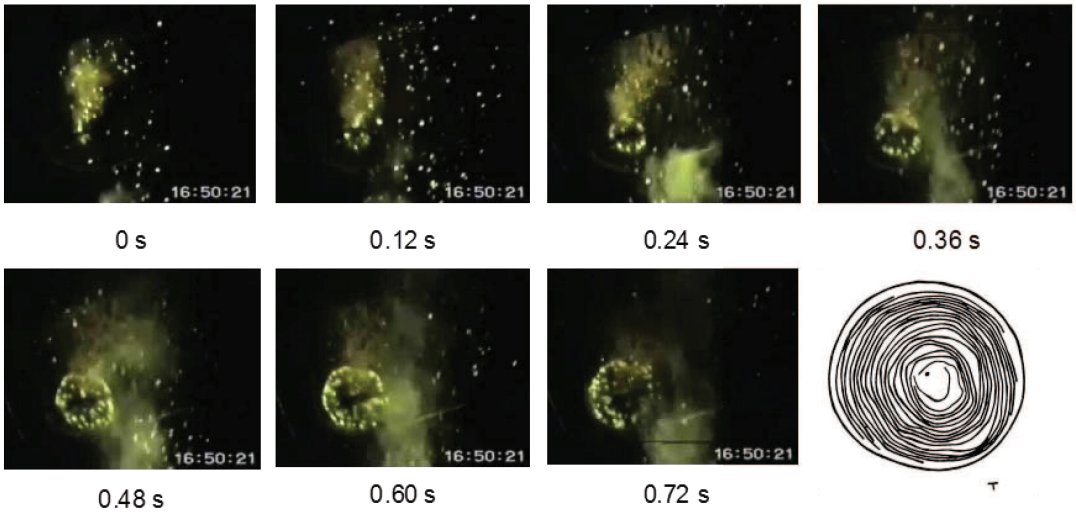

FIG. 7: Example of the experimental combustion front propagation in the stoichiometric thermite mixture. Some of the video frames were omitted for simplicity. On the right bottom are presented the corresponding combustion propagation profiles in the interval 0–0.76 s (one profile per each 0.04 s; the external profile is the circular box confinement; T indicates the direction of positioning of thermocouples).

TABLE 2: General data for the simulation

$Q\|_{T_0}$ (J/kg)	T_0 (K)	P (Pa)	T_{igni} (K)	T_{react} (K)	R (m)	R_0 (m)
5322746	298.15	101325	2300	1200	0.025	0.0015
Z (m)	τ (s)[a]	T' (K)[a]	Δr (m)		υ_{air0}[b]	
0.0015	0.1	1000	1×10^{-5}		0.392	
α_{A}	α_{B}	α_{C}	α_{D}	ω_{A}	ω_{B}	
–1	–0.33792	0.69943	0.63848	0.747	0.253	

[a] Time and temperature normalization constants

[b] Experimental mean porosity of the samples

TABLE 3: Numerical implementation conditions for 1D simulations

RKF45 tols.	Algorithm tol.		Finite diff. approximations	First-level grid uniform;
	β_1	β_2		
1×10^{-6}	1×10^{-1}		**centered; 5 nodes**	**40 intervals**
Criterion	Derivative		Routine	Interpolation
C2	first		gridgen1	cubic splines; seven nodes
Time step	Spatial derivative scheme			Max. refinement level
1×10^{-3}	Finite differences; centered five nodes			2

in a better fit to the experimental stationary combustion propagation velocity (see Section 3). Low variations in the predicted velocity ($\sim$ 1 mm/s, which is less than the experimental error) were observed with step changes of 10,000 kg·m^{-3}·s^{-1} in this constant.

The numerical algorithm is able to follow the thermal and mass propagation waves rather efficiently as the high-mesh activity zones accompany the movement of the steep fronts. Therefore, we conclude that the adaptive method is suitable to simulate propagation in uniform mixing conditions.

Additionally, the propagating velocity tends to a constant value at most of the radial domain and is proportional to the value of the kinetic constant, as would be expected (see Fig. 10). The behavior of the local velocities observed in experimental tests [see example in Fig. 10(a)] is well followed by the predicted radial velocity [Fig. 10(b)]. The main difference is noted in the outer boundary region ($r = R$), where the predicted radial velocity increases, and this was not detected in experimental conditions. This is possibly caused by a boundary condition effect.

In experimental conditions, for the initiation of the charges, an instantaneous discharge of a large amount of energy is introduced in the ignition channel (in the central region), which leads to an elevation of the local temperature in this region. Although this temperature effect was not directly measured, it is confirmed by the higher combustion velocity that is achieved in lower radii [exper-

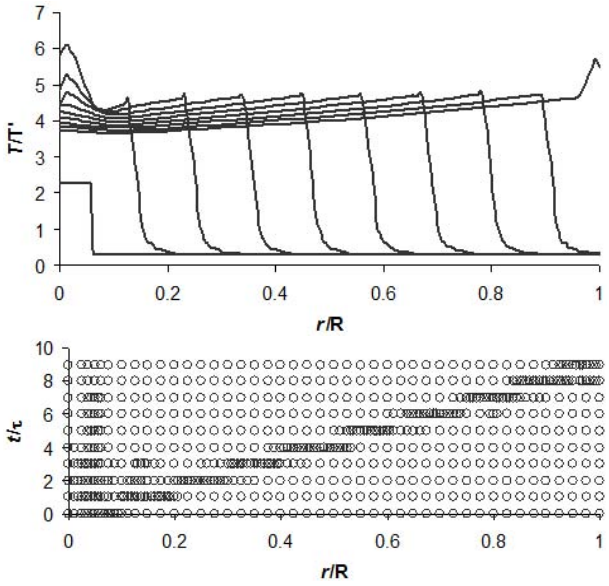

FIG. 8: Thermal wave 1D propagation for K = 80,000 kg·m^{-3}·s^{-1}. Time gap between profiles – 0.1 s.

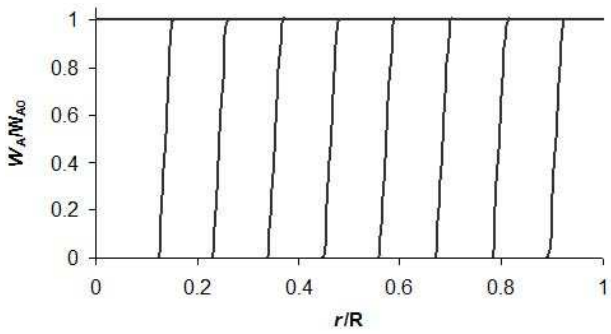

FIG. 9: Mass wave 1D propagation for K = 80,000 kg·m^{-3}·s^{-1}. Time gap between profiles – 0.1 s.

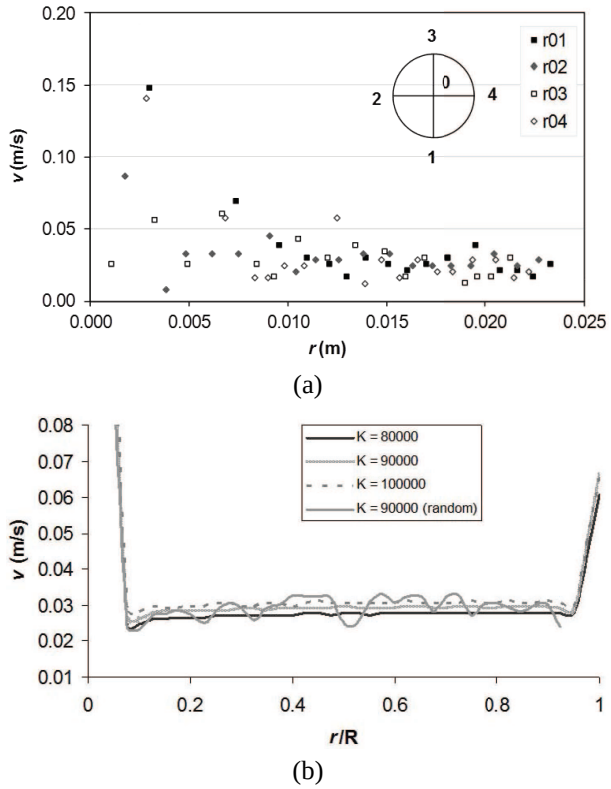

FIG. 10: (a) Radial combustion velocities obtained experimentally in four perpendicular axes of one of the samples; **(b)** calculated wave propagation velocity spatial profiles.

imental: Fig. 10(a)]. This higher velocity is also observed in the 1D simulation, as can be seen in Fig. 10(b). In addition, the referred temperature effect is also visible in the thermal wave profiles at early stages in Fig. 8 (t = 0.1–0.3 s).

Concerning the predicted combustion temperature (higher value on the thermal wave front of Fig. 8), it is higher than the experimental mean value (see Section 4). This is justified by the heat losses due to the spraying of products away from the combustion system and by the incompleteness of the reaction, observed experimentally (Durães et al., 2006a, 2007, Durães, 2007) and not considered in the model.

The introduction of randomly distributed reactant profiles, as effectively occurs in the experimental mixtures [see Fig. 10(a)], originates visible perturbations in the velocity evolution profile, as can be observed in Fig. 10(b). The example shown in this figure corresponds to initial Fe_2O_3 and Al profiles randomly generated by a procedure described in Brito et al. (2007), in similar conditions for a 41 node uniform mesh (see Fig. 11). It is visible that the profile is significantly affected by the nonhomogeneity of the initial reaction media, promoting more instability in the thermal wave propagation. The velocity profile shows evident oscillations around the average reference value, with no definition of an asymptotic value. The simulated profiles are clearly more realistic when compared with experimental propagation results of Fig. 10(a). This suggests that 1D radial propagation experimental variability can be at least partially explained by nonuniform mixing of reactants.

5.2 2D Model

Now we simulate the 2D system using the numerical conditions resumed in Table 4.

In a first approach we tested the uniform mixing reagent conditions. The numerical results obtained for K = 80,000 kg· m^{-3}·s^{-1} at three time instants (t = 0.1 s, t = 0.45 s, t = 0.8 s) are given in Fig. 12. We conclude

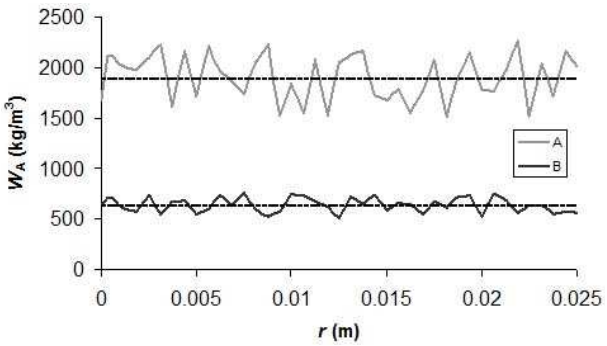

FIG. 11: Initial mass concentration of randomly generated profiles for A: Fe_2O_3 and B: Al.

TABLE 4: Numerical implementation conditions for 2D simulations

RKF45 *ATol*	**Algorithm tol.**		**Finite diff. approximations**	**First level dyadic grid uniform;**
	β_1	β_2		
1×10^{-5}	1×10^{-1}		**centered; five nodes**	**2^5 intervals in *r* and 2^3 in ϕ**
Criterion	Derivative		Routine	Interpolation
C52/C2	first		gridgen6	cubic splines; seven nodes
Time step	Spatial derivative scheme			Max. refinement level
1×10^{-3}	Finite differences; centered five nodes			2 in *r*; 0 in ϕ

that the algorithm does not seem to have any problem in dealing with the selected problem. Each radial propagation profile is very similar to the correspondent 1D profile, since the angular propagation is rather residual in these circumstances. This is experimentally confirmed by the observed circularity of the obtained combustion front propagation profiles (i.e., for a given profile, the front is nearly in the same radius position for all directions), as seen in Fig. 7. In addition, the light intensity emitted by the combustion front is almost the same in the major part of the profiles and for all directions, showing that the front does not exhibit high-temperature variations. This is also confirmed by the nearly stationary temperature registered by the two thermocouples located in different radii positions (see Durães et al., 2006a).

Finally, we have performed the 2D simulation using the randomly generated profiles shown in Fig. 11 in eight different propagation directions, uniformly distributed. The obtained thermal wave results are presented in Fig. 13. The registered oscillations in the temperature profiles follow the same trends observed for the 1D results and the experimental results, confirming that the 2D approach does not significantly affect the simulation performance. A similar strategy to this variation of concentrations can be used in the future to replicate more sophisticated nonuniformities in the reactant medium that are usually observed in experimental conditions, such as the local lack of reactants due to the presence of an obstacle, density variations, and thickness variations, among others.

6. CONCLUSIONS

An adaptive numerical algorithm that conjugates a "method of lines" (MOL) strategy based on finite differences space discretizations, with a collocation scheme based on increasing level dyadic grids, is applied for the solution of the thermite combustion propagation problems.

The particular integration method proves to cope satisfactorily with the steep traveling thermal wave in 1D and 2D spatial domains, either for trivial uniform mixing conditions, as for nonhomogeneous reactant mixing, which intends to replicate realistically observed experimental conditions.

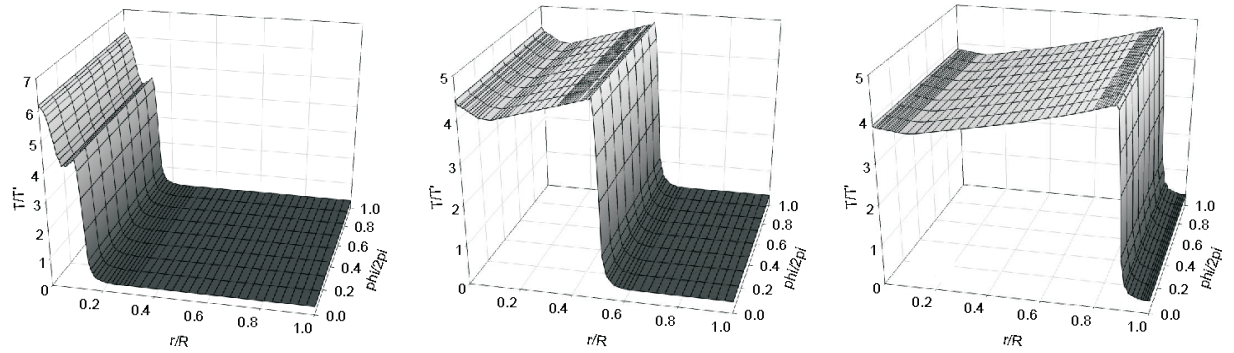

FIG. 12: Thermal wave 2D propagation for K = 80,000 kg·m^{-3}·s^{-1} and uniform mixing conditions: **(a)** t = 0.1 s, **(b)** t = 0.45 s, **(c)** t = 0.8 s.

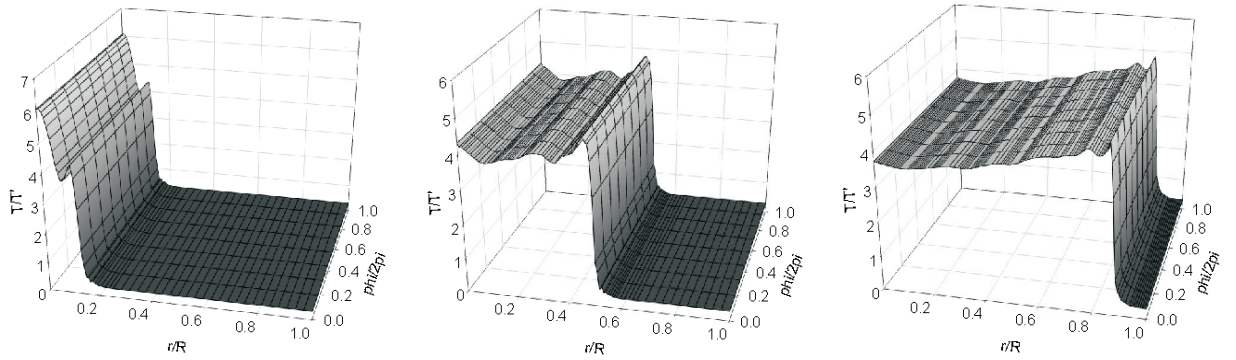

FIG. 13: Thermal wave 2D propagation for K = 80,000 kg·m^{-3}·s^{-1} and nonuniform mixing of reactants: **(a)** t = 0.1 s, **(b)** t = 0.45 s, **(c)** t = 0.8 s.

REFERENCES

Alves, M. A., Oliveira, P. J., and Pinho, F. T., A convergent and universally bounded interpolation scheme for the treatment of advection, *Int. J. Numer. Meth. Fluids*, vol. **41**, no. 1, pp. 47–75, 2003.

Bowen, C. R. and Derby, B., Finite-difference modelling of self-propagating high-temperature synthesis of materials, *Acta Metall. Mater.*, vol. **43**, no. 10, pp. 3903–3913, 1995.

Brito, P. M. P., *Métodos numéricos adaptativos para a resolução de modelos multidimensionais em Engenharia Química*, Ph.D. Thesis, Faculty of Sciences and Technology of University of Coimbra, 2010.

Brito, P., Durães, L., Campos, J., and Portugal, A., Simulation of Fe_2O_3/Al combustion: Sensitivity analysis, *Chem. Eng. Sci.*, vol. **62**, no. 18-20, pp. 5078–5083, 2007.

Brito, P., Durães, L., Campos, J., and Portugal, A., Modelling and Simulation of Fe_2O_3/aluminum thermite combustion, *CHEMPOR 2005, Proc. of 9th International Chemical Engineering Conference*, pp. 157–158 (and CD-ROM), 2005.

Brito, P., Durães, L., Campos, J. A., and Portugal, A., Aplicação de Métodos Adaptativos para a Simulação de Processos de Combustão, *CMCE 2004, Proc. of Congresso de Métodos Computacionais em Engenharia*, p. 472 (and CD-ROM), 2004.

Cruz, P., Alves, M. A., Magalhães, F. D., and Mendes, A., Solution of Hyperbolic PDEs using a stable adaptive multiresolution method, *Chem. Eng. Sci.*, vol. **58**, no. 9, pp. 1777–1792, 2003.

Darwish, M. S. and Moukalled, F., Normalized variable and space formulation methodology for high-resolution schemes, *Numer. Heat Transfer, Part B*, vol. **26**, no. 1, pp. 79–96, 1994.

Driscoll, T. A. and Heryudono, A. R. H., Adaptive residual subsampling methods for radial basis function interpolation and collocation problems, *Comput. Math. Appl.*, vol. **5**, no. 6, pp. 927–939, 2007.

Durães, L., Campos, J., and Portugal, A., Radial combustion propagation in iron(III) oxide/aluminum thermite mixtures, *Propell. Explos. Pyrotechnic.*, vol. **3**, no. 1, pp. 42–49, 2006a.

Durães, L., Brito, P., Campos, J., and Portugal, A., Modelling and simulation of Fe_2O_3/aluminum thermite combustion: Experimental validation, in *Computer Aided Chemical Engineering*, Marquardt, W. and Pantelides, C., eds., vol. **21A**, Amsterdam: Elsevier, pp. 365–370, 2006b.

Durães, L., Costa, B. F. O., Santos, R., Correia, A., Campos, J., and Portugal, A., Fe_2O_3/aluminum thermite reaction intermediate and final products characterization, *Mater. Sci. Eng. A*, vol. **465**, no. 1-2, pp. 199–210, 2007.

Durães, L., *Study of the reaction between iron(iii) oxide and aluminum and evaluation of its energetic potential*, Ph.D. Thesis, Faculty of Sciences and Technology of University of Coimbra, 2007.

Fornberg, B., Generation of Finite difference formulas on arbitrarily spaced grids, *Math. Comput.*, vol. **51**, no. 184, pp. 699–706, 1988.

Gonzo, E. E., Estimating correlations for the effective thermal conductivity of granular materials, *Chem. Eng. J.*, vol. **90**, pp. 299–302, 2002.

Jakob, M., *Heat Transfer*, New York: John Wiley & Sons, 1949.

Makino, A., Fundamental aspects of the heterogeneous flame in the self-propagating high-temperature synthesis (SHS) process, *Prog. Energy Combust. Sci.*, vol. **27**, pp. 1–74, 2001.

Moore, J. J. and Feng, H. J., Combustion synthesis of advanced materials: Part II. Classification, applications and modelling, *Prog. Mater. Sci.*, vol. **39**, pp. 275–316, 1995.

Mukasyan, A. S., Hwang, S., Sytchev, A. E., Rogachev, A. S., Merzhanov, A. G., and Varma, A., Combustion wave microstructure in heterogeneous gasless systems, *Combust. Sci. Technol.*, vol. **115**, pp. 335–353, 1996.

Mukasyan, A. S., Rogachev, A. S., and Varma, A., Mechanisms of reaction wave propagation during combustion synthesis of advanced materials, *Chem. Eng. Sci.*, vol. **54**, pp. 3357–3367, 1999.

Petzold, L. R., *A description of DASSL: A differential/algebraic system solver*, Sandia Technical Report no. 82-8637, 1982.

Raymond, C. S., Shkadinsky, K. G., and Volpert, V. A., Gravitational effects on liquid flame thermite systems, *Combust. Sci. Technol.*, vol. **131**, pp. 107–129, 1998.

Santos, J. C., Cruz, P., Magalhães, F. D., and Mendes, A., 2-D wavelet-based adaptive-grid method for the resolution of PDEs, *AIChE J.*, vol. **49**, no. 3, pp. 706–717, 2003.

Schiesser, W. E., *The numerical Method of Lines: Integration of Partial Differential Equations*, San Diego: Academic Press, 1991.

Shampine, L., Watts, H., and Davenport, S., Solving non-stiff ordinary differential equations—The state of the art, *SIAM Rev.*, vol. **18**, no. 3, pp. 376–411, 1976.

Shkadinsky, K. G., Shkadinskaya, G. V., and Matkowski, B. J., Gas-phase influence on quasisteady "liquid flames" in gravitational fields, *Combust. Sci. Technol.*, vol. **157**, pp. 87–110, 2000.

Shkadinsky, K. G., Shkadinskaya, G. V., and Volpert, V. A., Stability of "liquid flame" combustion waves, *Chem. Eng. Sci.*, vol. **52**, no. 9, pp. 1415–1428, 1997.

Tavman, I. H., Effective thermal conductivity of granular porous materials, *Int. Commun. Heat Mass Transfer*, vol. **23**, no. 2, pp. 169–176, 1996.

Vande Wouwer, A., Saucez, Ph., and Schiesser, W. E., eds., *Adaptive Method of Lines*, Boca Raton: Chapman & Hall/CRC Press, 2001.

Varma, A. and Lebrat, J.-P., Combustion synthesis of advanced materials, *Chem. Eng. Sci.*, vol. **47**, no. 9-11, pp. 2179–2194, 1992.

Varma, A., Rogachev, A. S., Mukasyan, A. S., and Hwang, S., Complex behaviour of self-propagating reaction waves in heterogeneous media, *Proc. Natl. Acad. Sci. U. S. A.*, vol. **95**, pp. 11053–11058, 1998.